A B$_4$C–Silicon Target for the Detection of Neutrino Interactions

G. Barichello[a], A. Cervera–Villanueva[b], D.C. Daniels[c], E. do Couto e Silva[b],
L. Dumps[b], M. Ellis[d], D. Ferrère[b,1], J.J. Gómez–Cadenas[b], C. Gößling[e],
M. Gouanère[f], J.A. Hernando[g,2], W. Huta[b], J.M. Jiménez[b], J. Kokkonen[b],
V.E. Kuznetsov[h,3], L. Linssen[b], J. Long[b,4], B. Lisowski[e,5], A. Lupi[i], Ö. Runolfsson[b],
B. Schmidt[e,3], F.J.P. Soler[d], D. Steele[j], M. Stipčević[k], M. Veltri[i], D. Voillat[b].

a. University of Padua, Padua, Italy.
b. CERN, Geneva, Switzerland.
c. Harvard University, Cambridge, MA, USA.
d. University of Sydney, Sydney, Australia.
e. Dortmund University, Dortmund, Germany.
f. LAPP, Annecy, France.
g. University of Valencia, Valencia, Spain.
h. Joint Institute for Nuclear Research, Dubna, Russia.
i. University of Urbino, Urbino and INFN, Florence, Italy.
j. University of Lausanne, Lausanne, Switzerland.
k. Rudjer Bošković Institute, Zagreb, Croatia.

Abstract

This note describes the construction of a target for neutrino interactions composed of passive boron carbide plates interleaved with silicon microstrip detectors. The target contains four layers of passive material with a total mass of 45 kg and 600 single–sided silicon microstrip detectors with a total surface of 1.14 m^2 distributed over five layers. It is installed in the NOMAD spectrometer at the CERN SPS neutrino beam. During the 1997 run about 8000 ν_μ charged current interactions were estimated to have occurred in the target. For these events it will be possible to perform a precise measurement of both vertex and kinematical variables. This will provide invaluable experience towards the construction of a future large scale silicon tracker for neutrino oscillation experiments.

Submitted to Nuclear Instrumentation and Methods.

---

[1]Now at University of Geneva, Geneva, Switzerland.
[2]Now at University of California at Santa Cruz, California, USA.
[3]Now at CERN, Geneva, Switzerland.
[4]Now at University of Colorado, Colorado, USA.
[5]On leave of absence from Institute of Electron Technology, Warsaw, Poland.

1 Introduction

One of the most interesting current problems in particle physics and cosmology is the possibility that neutrinos have non-vanishing masses and that there are oscillations among the different families. At present, two experiments, CHORUS and NOMAD [1, 2], are searching for the exclusive $\nu_\mu(\nu_e) \leftrightarrow \nu_\tau$ oscillation modes in the CERN-SPS neutrino beam. Furthermore, a new generation of experiments to search for $\nu_\mu(\nu_e) \leftrightarrow \nu_\tau$ oscillations, with a sensitivity at least an order of magnitude larger than CHORUS and NOMAD, is being actively discussed [3, 4, 5, 6, 7, 8]. All these experiments are based on a target equipped with high resolution tracking detectors, capable of detecting the topological signature of the τ decays. The simplest possible design for such a target consists of a sandwich of passive, low–Z target material and high resolution sensors, i.e. microstrip silicon detectors as proposed in [3]. This paper presents a prototype target based on this design. A large–size neutrino oscillation experiment with typical target mass of 2 tons will require about 50 m^2 of silicon detectors. An additional improvement on the vertex capabilities can be achieved by replacing the passive target plates by nuclear emulsion as proposed in [4, 5, 6, 7].

The running conditions of a neutrino experiment imply low rates, low occupancies and negligible radiation levels. This permits the use of low–noise readout chips for the silicon detectors, based on shaping times of about 3 μs. The main challenge consists in building large silicon surfaces covering beam areas of about 1.5 $\times$ 1.5 m^2 at low cost. To maximize the detector acceptance and to minimize the number of readout channels, we have opted for 72 cm long detector modules. For the passive material boron carbide was selected for its low–Z constituents combined with its high density.

To test the combination of the precision vertex measurement of the target with measurements of kinematical variables, the target is installed in the NOMAD spectrometer at the CERN SPS neutrino beam.

The organization of this note is as follows. Section 2 describes the main properties of the target and the NOMAD spectrometer. Section 3 discusses the test procedures and results for the silicon detectors. In section 4 the ladder construction is described. The results from ladder testing are summarized in section 5. Section 6 gives an overview of the survey and its main results. Section 7 describes the mechanical support structure and cooling of the detector. Section 8 presents an overview of the electronics. The data acquisition system is described in section 9. The laser alignment system is briefly mentioned in section 10. In section 11 the conclusions are presented.

2 NOMAD–STAR

The NOMAD apparatus shown schematically in Fig. 1 measures and identifies the electrons, muons, photons and hadrons produced in neutrino interactions. The active target in NOMAD is a set of drift chambers with a fiducial mass of about 2.7 tons. Measurements of the kinematical properties of neutrino interactions produced in this target allow the identification of possible τ candidates [2]. However, the drift chamber resolution is not sufficient to provide τ identification based on topological criteria.
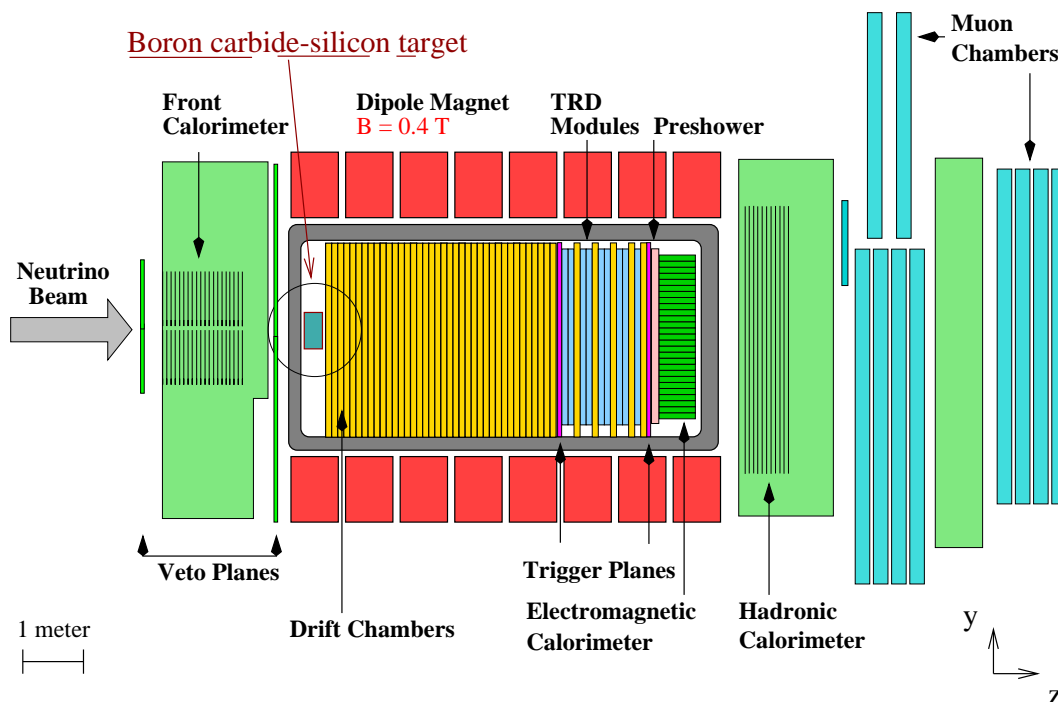

Figure 1: The NOMAD detector with the boron carbide–silicon target (NOMAD–STAR).

The target shown in Fig. 2 was installed upstream of the first NOMAD drift chamber. It follows the concept of a passive target followed by sensitive layers proposed in [3]. It consists of four layers of boron carbide (B_4C) interleaved with layers of single–sided silicon microstrip detectors. An additional layer of silicon detectors is added downstream for better track reconstruction.

The boron carbide plates with total mass of 45 kg serve as passive material for the neutrino interactions. Each of the four plates has dimensions of 72×31.5
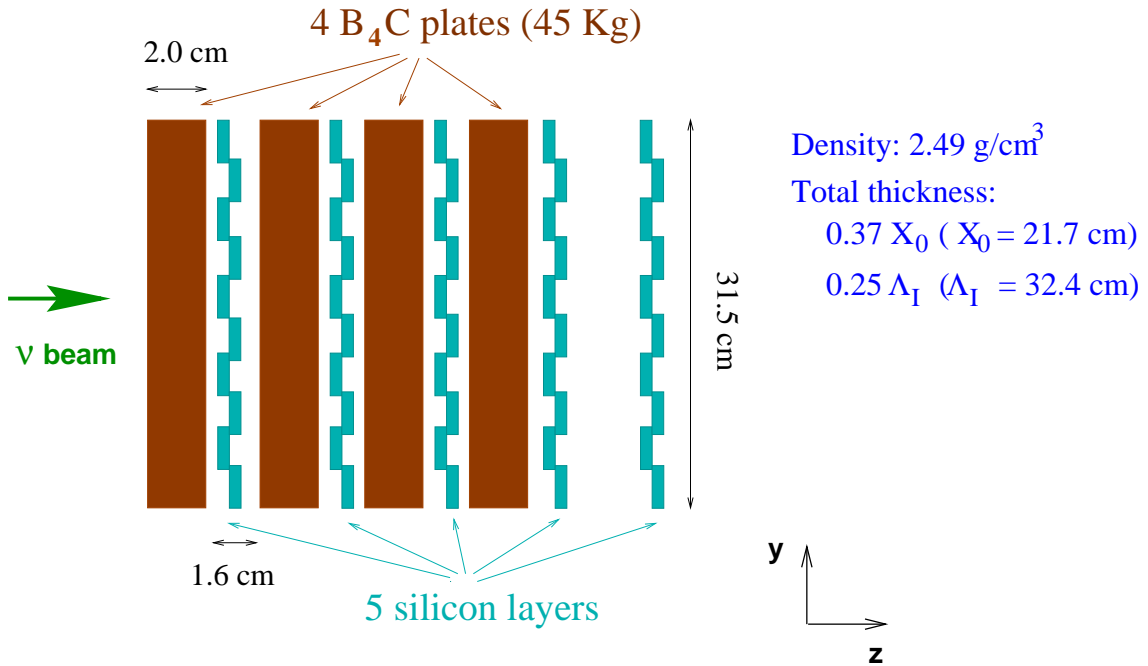
Figure 2: Schematic of the side view of the silicon target.

$\times$ 2 cm^3. Boron carbide provides the best compromise between high density and long radiation length for low Z materials. The five layers of silicon microstrip detectors[6] have an active surface of 1.14 m^2. As shown in Fig. 3 each active layer consists of 10 overlapping modules (ladders) assembled with twelve silicon microstrip detectors. The silicon microstrip detectors are of the same type as those used in the DELPHI experiment [9]. These are single–sided, AC coupled, FOXFET biased [10] passivated with silicon oxide. The strip and readout pitch are 25 μm and 50 μm, respectively. Each detector has 641 readout strips, but to match the channel pitch of the readout chips, 640 strips are read out. The strips are oriented in the direction parallel to the NOMAD magnetic field.

The performance of these silicon ladders in terms of signal–to–noise ratio, hit finding efficiency and spatial resolution has been described elsewhere [11].

An example of a reconstructed ν_μ charged current interaction occurring in the target is depicted in Fig. 4.

3   Detector Testing

The silicon microstrip detectors were tested for:

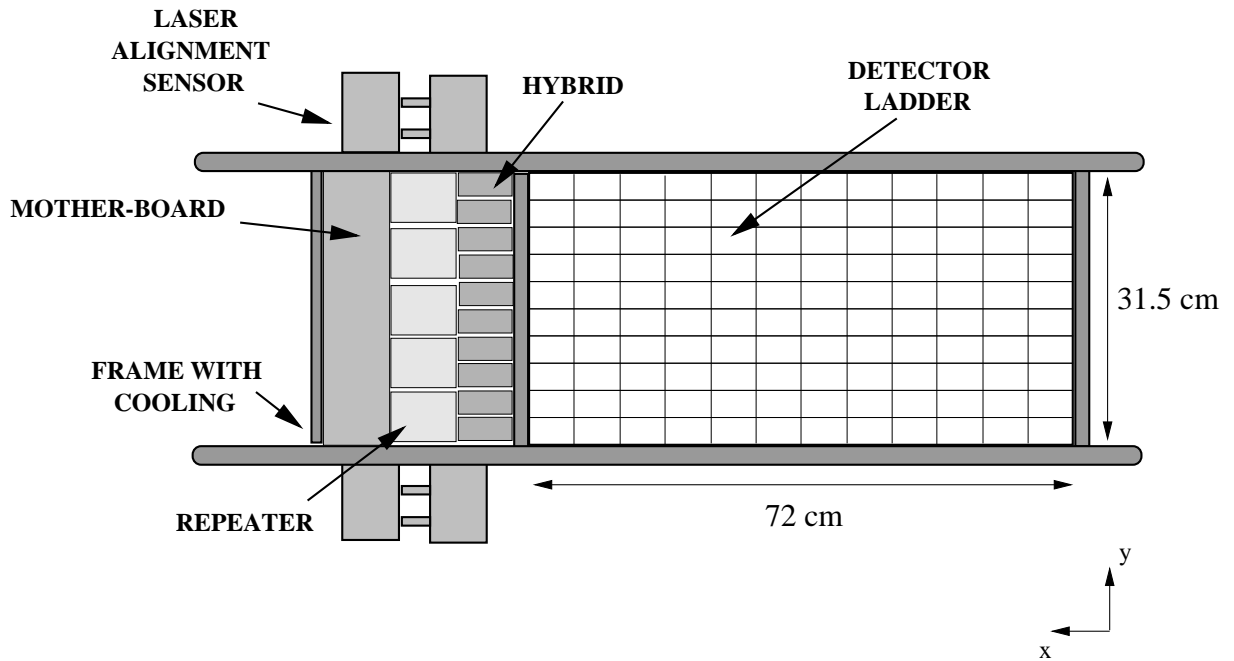[6]Manufactured by Hamamatsu Photonics, Japan.

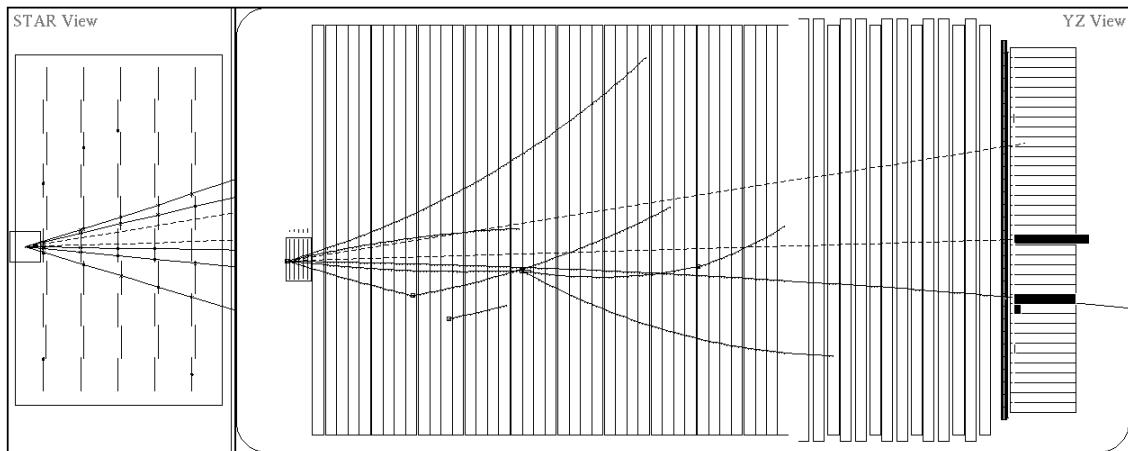Figure 3: Individual silicon layer with 10 ladders and 12 detectors per ladder.

Figure 4: Reconstructed ν_μ charged current interaction inside the B_4C–silicon target (expanded view of the target is shown on the left).

- the number of defective channels (short–circuited or interrupted strips),

- leakage current.

3.1 Visual Inspections

To minimize risks of damage, detectors were only visually inspected.

A probe station with a high magnification microscope and a CCD camera were used to inspect detector scribe lines and edges. Strips were also checked for short–circuits or interrupted connections, and implants and metalization were checked for defects. Every detector was inspected twice. The first visual inspection mapped the detector defects and the second inspection was used as a cross–check. All major defects were photographed. From a total of 623 detectors, 19 were considered to have processing errors[7], such as changes in oxide thickness or interrupted floating strips.

To test for short circuits through the oxide one needs to probe the individual strips. This information was obtained during wire bonding [12]. Since we daisy–chain 12 detectors in a module (ladder) we had to ensure that the number of defective channels was as small as possible. An average of 0.2 (0.03%) defective strips were found per detector.

3.2 Leakage Current Tests

NOMAD–STAR specifications required leakage currents to be less than 5 μA. To test this, detectors were placed in light–tight probe stations in a climatized room.

Each detector was reverse–biased and the bias line was protected with 100 kΩ resistors to prevent overcurrents. Detector bias pads were contacted with probe needles. A power supply was used to change the gate–drain voltage difference (V_{GD}). Gate and bias currents were monitored independently.

A short term leakage current test was performed for different values of gate–drain voltage. No detector was rejected due to gate currents. For a sample of 30 detectors, no significant variations in the leakage current were measured for floating or grounded gates. Therefore in all subsequent measurements the gate was left floating.

Detectors were biased at about 70 V. Typical tests consisted of continuously monitoring the leakage currents of the detectors for 18 to 24 hours. Thermistors were also attached to the measuring set–up. The Data Acquisition System (DAQ) consisted of a custom–made VME module and a CPU MVME147 connected to a computer.

Figure 5a shows the distribution of the measured leakage current for 620 detectors held at a bias voltage of about 70 V. In Fig. 5b only detectors with leakage current below 300 nA are displayed, corresponding to 92% of the total

---

[7]However, 13 of these detectors had to be used for ladder assembly (see Table 1).

Type	Quantity	Quantity (%)
Good quality detectors	600	96.3
Serious processing errors	6	1.0
Unstable leakage current after ladder assembly	5	0.8
Losses due to accident	4	0.6
Runaway leakage current	3	0.5
Unstable leakage current after cleaning	3	0.5
Patterning defects after cleaning	2	0.3
Total	623	100.0

Table 1: Summary of detector statistics.

number of detectors. Out of 623 detectors only 3 could not hold the bias voltage and had runaway leakage currents ($> 10 \ \mu A$).

A particular problem appeared during wire bonding. The metalized bond pads at the first strip close to the FOXFET gate end for some detectors had a different color (brown) than expected (silver). This was related to an accidental spill of silicon oxide on the bond pads during dicing [13]. The bondability of the brown colored detectors was poor due to large variations in the bonding parameters. As a consequence, a significant number of bond wires were lost during bonding. In addition, the metal on the bond pad could be scraped away too easily.

In an attempt to solve this problem, we developed a technique to improve the quality of bonding[8]. For a wire that would break in the 90° bend rather than at the end of the weld spot, the next bond cycle would be completed with no wire under the wedge. To avoid that, 1/3 of the second bond was placed outside the pad border forcing the wire to break at the border.

The tight time scale of the project did not allow for any delay to replace the brown–colored detectors. Therefore they were washed in a commercial cleaning machine for printed circuits. Leakage current tests and visual scans were done before and after washing. Table 1, shows a final detector yield of 96.3% and itemizes the detector losses.

---

[8]A detailed description on the wire bonding can be found elsewhere [12].
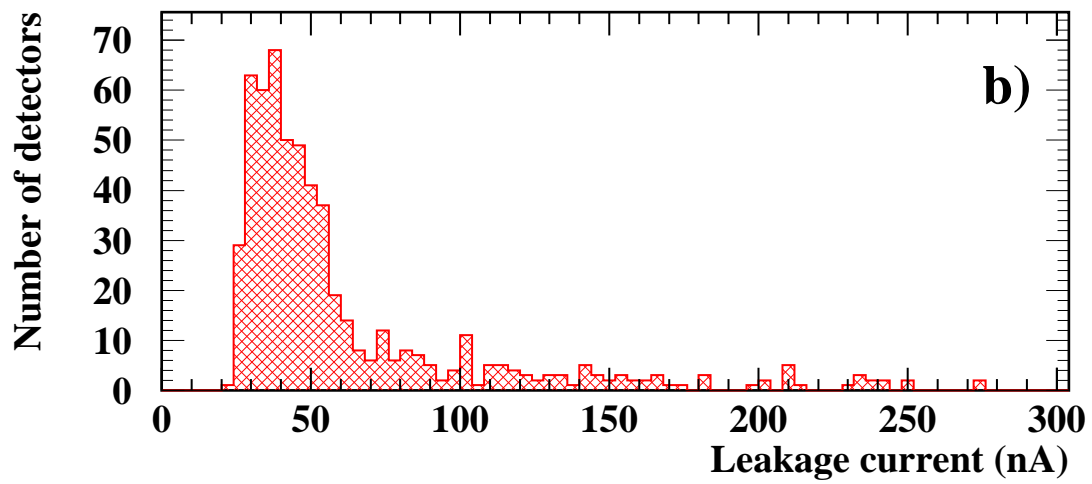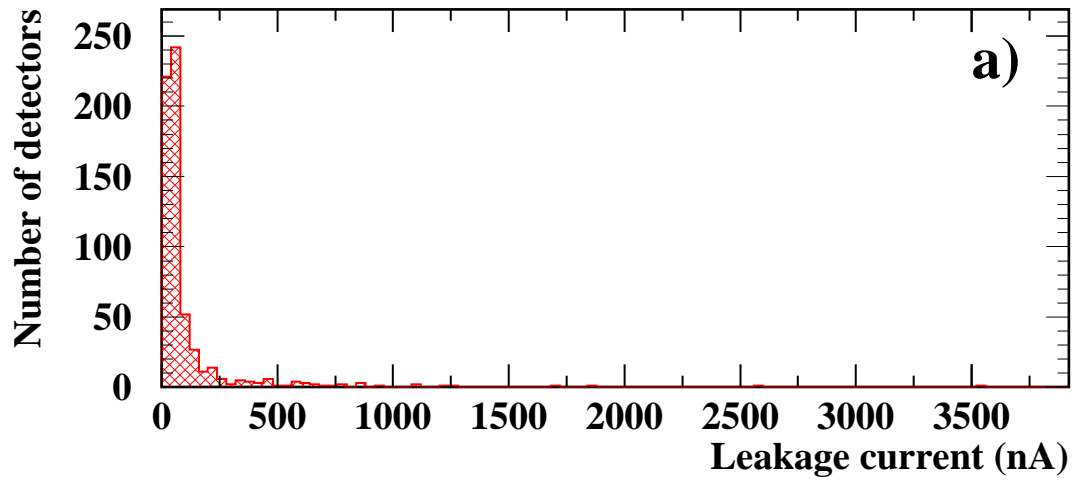
Figure 5: Leakage current distributions for: a) all detectors: and b) only detectors with leakage current smaller than 300 nA.

4   Ladder Construction

4.1   Overview

To minimize the number of readout channels and the dead regions in the sensitive area, NOMAD–STAR is based on very long ladders of silicon detectors. Therefore it requires a mechanical support which guarantees rigidity and stability over the total length of the ladder.

4.2   Ladder Assembly

Figure 6 illustrates the assembly of a ladder. Twelve silicon detectors are glued to a thin kapton foil which electrically isolates them from a conducting carbon fiber back bone. The carbon fiber back bone is made of two rectangular sections of carbon fiber. Each of the sections is made of two rectangular rods of 2.5 mm thickness glued back–to–back. The beams are made of ten layers of carbon fiber prepeg impregnated with a thermoset resin[9]. The density of the material, once cured, is 1.53 g/cm^3 with a radiation length of about 30 cm. In practice, the carbon fiber back bone which has a total thickness of 5 mm, constitutes part of the radiator. It contributes to about 10% to the target mass and to about 15% of the radiation length.

One of the ends of the ladder is glued to an aluminum support that carries a hybrid printed circuit board, fixing and alignment holes. The readout chips are mounted on the hybrid board. At the opposite end, a gold–plated ceramic plate is glued to allow noisy channels to be grounded (see section 5). To compensate for thermal expansion the end piece at the far end of the ladder is allowed to move.

To test ladders after assembly (see section 5), twelve printed circuits are mounted on the backside. These circuits contain 10 MΩ resistors connected to the backplane of each detector. Therefore the leakage current for each detector can be measured separately. In addition, a capacitor is connected to the backplane of the detectors at the end of the ladder. A voltage step applied to this capacitor induces charge pulses in all strips for tests and calibration.

4.3   Assembly set–up, alignment and gluing

The equipment for assembling the detector ladders was designed and built to allow easy and fast production with a precision of approximately 5 μm. The set–up consisted of an X–Y table with a position display, a CCD camera and a line generator to produce reference marks on the monitor.

---

[9]The prepeg is manufactured by Stesalit Ltd., it contains unidirectionally aligned carbon fiber from Mitsubishi Chemical.
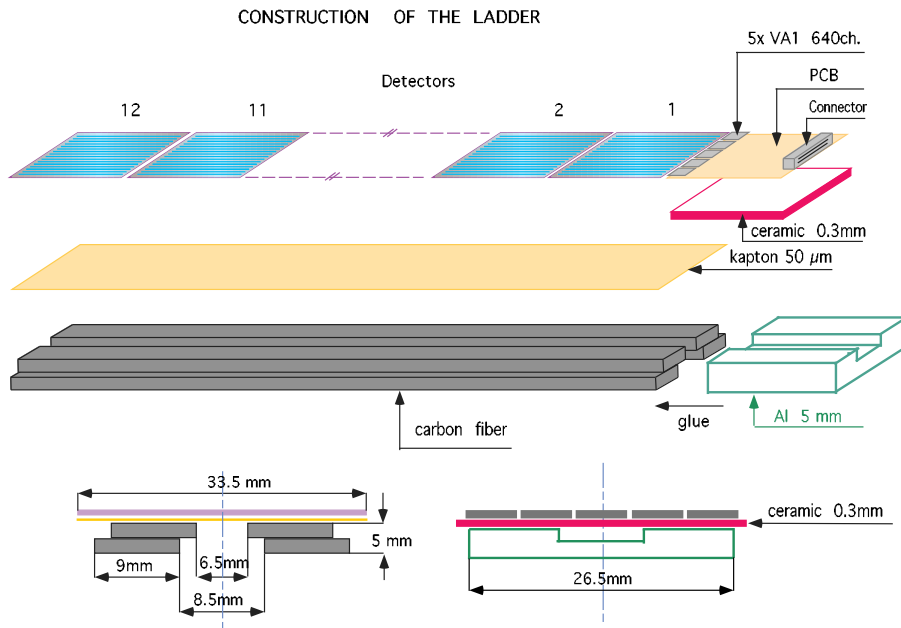
CONSTRUCTION OF THE LADDER

Figure 6: Schematical drawing of a ladder.

First, the kapton was glued to the carbon fiber using a thin continuous layer of glue. Special care was taken to avoid air bubbles in the glue. An epoxy was used to glue a previously tested hybrid. The position of the hybrid was determined by the alignment holes of the end pieces. After that, twelve detectors were glued with silicon glue[10] spread under the region where the bond pads are located and a spot of conductive "cold" glue was used to provide the biasing to the backplane. Detectors were aligned using reference dowel holes at both ends of the ladder. For both hybrid and detectors the gluing technique was a regular pattern of continuous dots, so that if needed, these elements could be easily removed from the ladder. Detectors with defective strips, were mounted at the far end of a ladder.

To prevent discharges in case of a large difference of potential between two detectors in a ladder, their longitudinal separation was approximately 200 μm. After gluing, the misalignment was about 10 μm. A thermal cycle of 100 °C for an hour was used to polymerize the glue and led to a misalignment as large as 30 μm.

---

[10]Manufactured by Dow Corning, Belgium.

5 Ladder Testing

Our testing programme consisted of measuring

- the response of the chips in a hybrid before ladder assembly,

- the total leakage current,

- the depletion voltage,

- noise and backplane charge distributions,

- the individual response of each channel with a laser beam.

Hybrids were tested and diagnosed before ladder assembly. The input calibration pulse of the VA1 chips was used to determine defective channels. Hybrids with more than two defective channels were rejected and the chips were replaced.

Before bonding the readout channels, the leakage current of the ladder was measured after connecting the backplane, drain and gate pads. The values were compared to those from the individual detector measurements. For every ladder test the leakage current was recorded so that its stability in time could be evaluated. For each ladder, a radioactive ruthenium source was used to measure
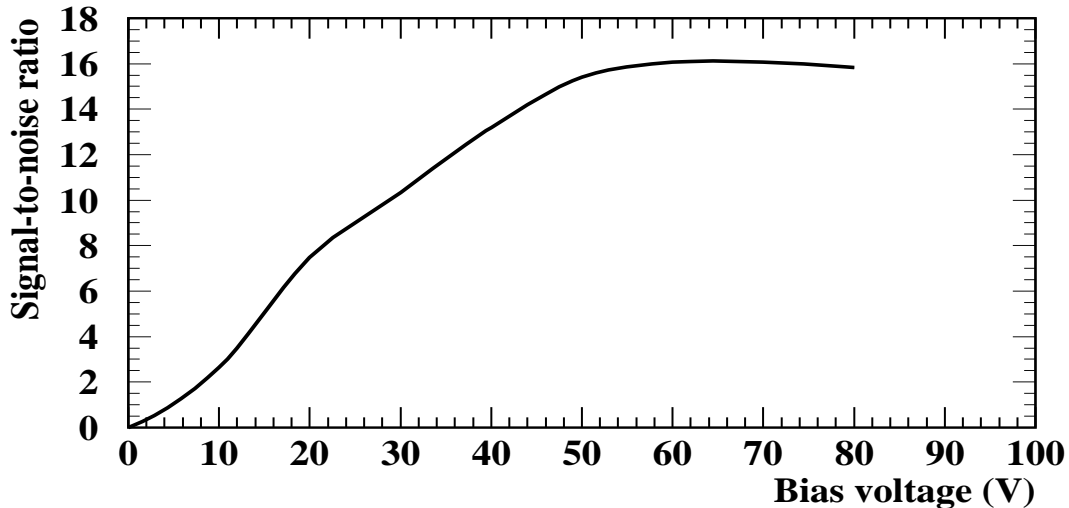

Figure 7: Signal–to–noise ratio versus bias voltage for a typical ladder.

the signal–to–noise ratio at different bias voltages. As illustrated in Fig. 7 the signal–to–noise ratio is constant after depletion. This measurement was used to

10

define the operational bias voltage of 60 V. For all ladders gate and drain pads were grounded.

For each ladder the sigma of the pedestal was calculated (noise) and the common–mode shift was evaluated on a chip–by–chip basis. In addition, a voltage step was applied across a capacitor connected to the backplane of one of the detectors at the end of the ladder. The charge induced in every strip was also recorded.
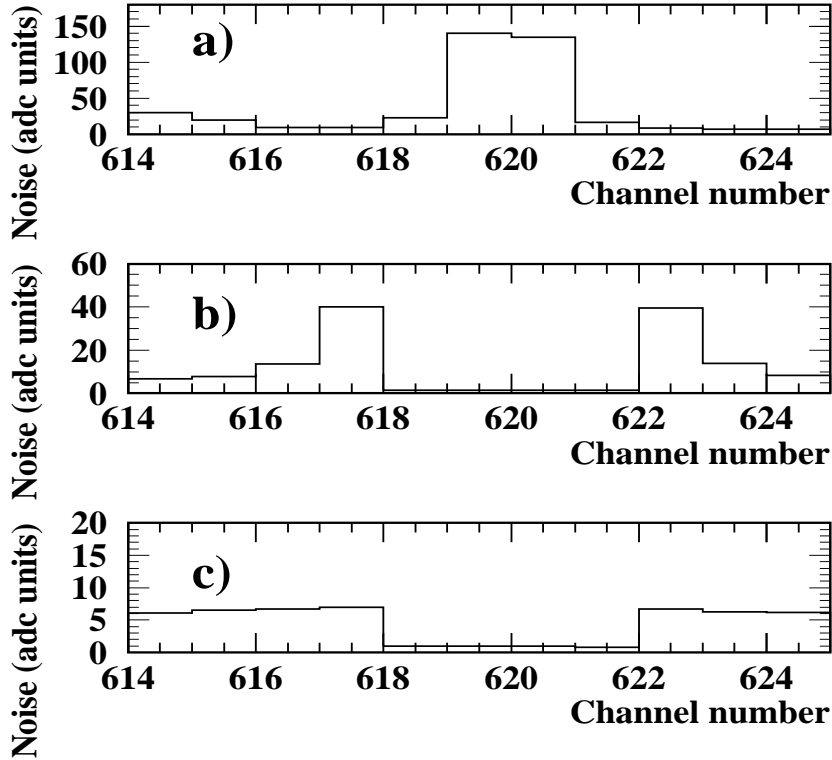

Figure 8: Noise for all channels of a typical ladder with a) very noisy strips, b) noisy strips removed c) noisy strips grounded.

A diode strip with high leakage current can lead to a significant increase in the noise. As shown in Fig. 8a a noisy strip may affect its neighbors. In Fig. 8b the noisy strips were disconnected from the readout end but the noise on its neighbors remained high. As shown in Fig. 8c the noise was further reduced when the strips disconnected at the readout end were connected to ground on the far end of the ladder.

Interrupted strips were identified by observing the reduction in the noise from the average value (see Fig. 9a). As shown in Fig. 9b this effect was confirmed
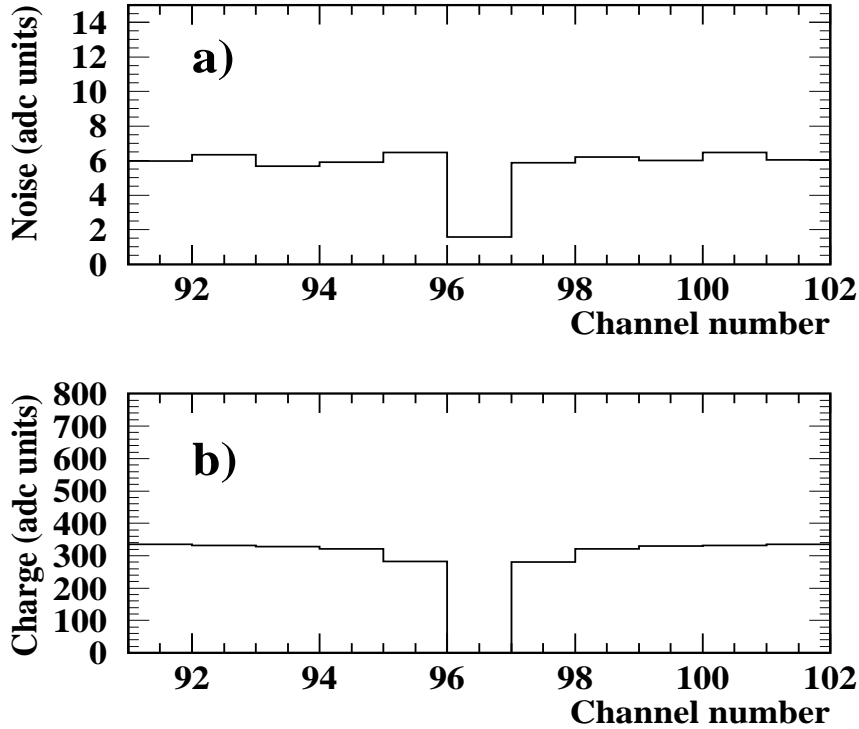
Figure 9: a) Noise, b) measured strip charges with backplane pulsing for a typical ladder with an interrupted strip.

with no charge collection for backplane pulsing. If this was due to missing bonds between detectors, bonds were then remade.

In a pair of short–circuited channels each channel is either saturated by a current offset or has a high noise corresponding to the low impedance of the other one. These arise from defects in processing or from imperfect bonding. As shown in Fig. 10a this effect was clearly seen in the noise distributions. To avoid that, bond wires were separated (Fig. 10b) or a bond was removed from one of the channels. In most cases a signal from an interrupted channel will be found in its neighbors.

5.1 Tests with a laser beam

Tests with a laser beam were devised as a powerful cross–check of the previous measurements on a strip–by–strip basis.

The set–up was placed inside a light–tight box and consisted of an infrared high–power pulsed laser diode, whose light was focused by a microscope. The microscope was mounted on a movable table driven by a step motor which allowed precise detector scanning in the direction perpendicular to the orientation of the strips. The entire system was mounted on a rail and could be moved by hand along the direction parallel to the strips allowing the positioning of the laser on
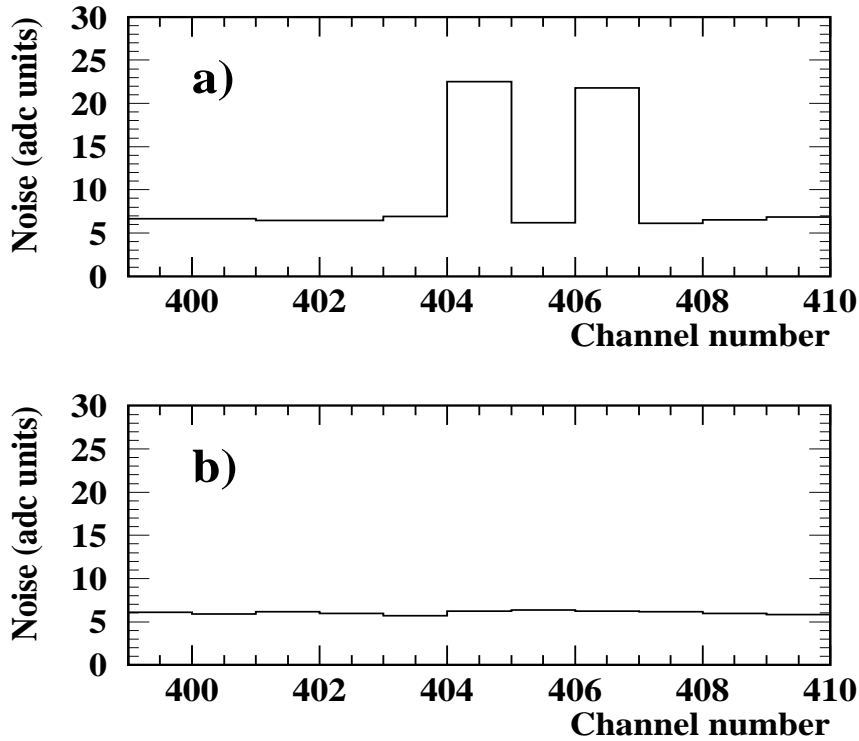
Figure 10: Noise for all channels of a typical ladder with a) shorted strips, b) shorted wires separated.

each of the twelve detectors of the ladder.

The laser has a wavelength of 904 nm and operated at a peak power of about 2 W with a maximum frequency of 125 Hz. Its short light pulse (about 40 ns) was sent through an optical fiber into the microscope ocular. The beam was focused onto a spot of approximately 20 μm on the surface of the silicon detector with a 50 μm readout pitch.

A typical scan of a ladder took about 100 minutes to be completed. For each ladder the closest and the farthest detector with respect to the hybrid were scanned. The two scans were compared to identify defective strips along the ladder. During the scan only the strip hit by the laser beam and the two nearest neighbors, and occasionally some noisy channel, will give a signal. At the end of each scan, mean and sigma values for signals and pedestals were calculated.

Fig. 11 shows the total charge collected by the strips versus laser position perpendicular to the orientation of the strips. The readout strip position is in the "valley". The observed reduction in the charge is due to the partial reflection of the laser light from the aluminum layer which covers the strip.
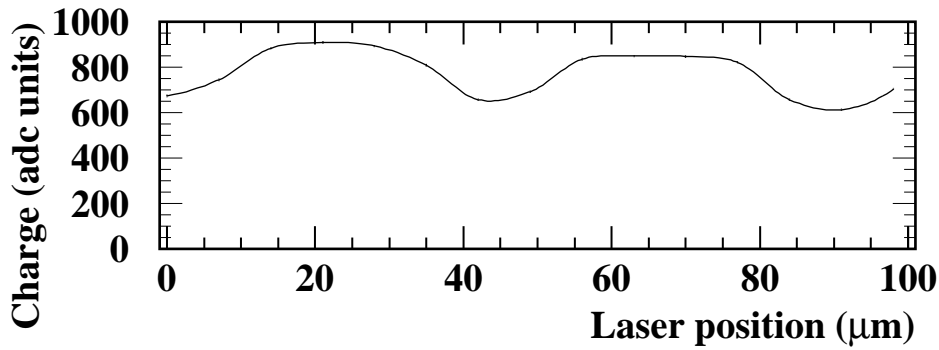
Figure 11: Total charge collected by the strips.

5.2 Ladder Repair

A readout chip or a silicon detector was replaced in case of failure or accidents. The readout chips were removed by softening the glue by blowing hot air or using a soldering iron. Detectors were removed by cutting the glue spots with a strip of kapton.

One of the problems identified after the ladder assembly, was a short–circuit of several bond wires. In principle, bond wires should oxidize with time and
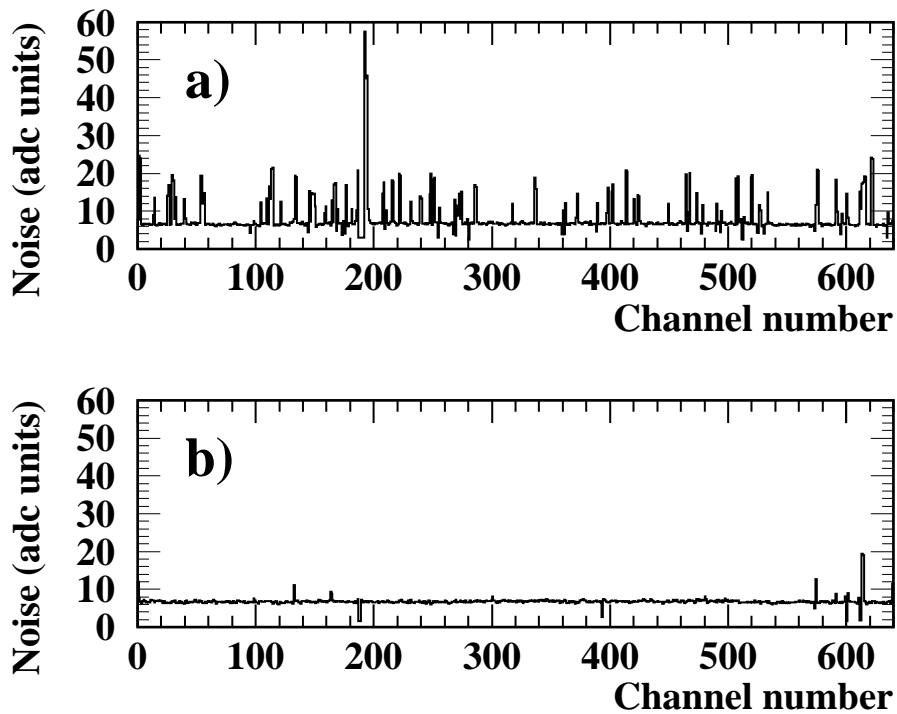

Figure 12: Noise for all channels of a typical ladder with: a) several short–circuited strips, b) short–circuited wires separated.

short–circuits should disappear even if bonding wires touch each other. Since many strips were short–circuited, the information from the laser test was not very useful. Bond wires were separated one by one with the aid of a needle. This was done for all ladders. The effect of separating the bonds to remove the short–circuits is illustrated in Fig. 12.

The summary of the ladder tests after repair is shown in Figs. 13a and 13b. Time constraint did not permit to fully debug all ladders which implied that some ladders had as much as 7% defective channels and high leakage currents. In spite of that, an average of 1.4% defective channels was obtained.
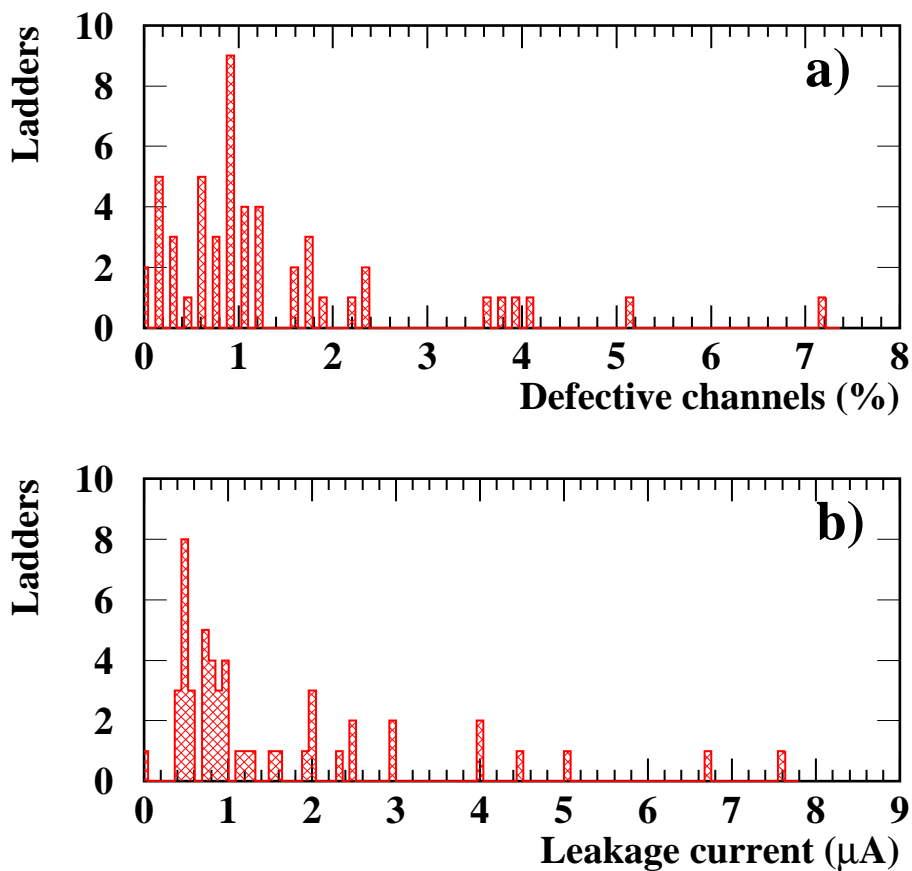

Figure 13: a) Percentage of defective channels for all ladders, b) leakage current for all ladders.

6 Ladder Survey

In order to have a position resolution of less than 10 μm in the direction perpendicular to the orientation of the strips, each layer had to be surveyed accurately. A full description of the survey can be found elsewhere [14].

The surveying was performed using a CCD camera with magnifying optics, mounted on a measuring table. As shown in Fig. 14, the silicon layer under survey was mounted vertically, facing the camera. The axes for the measurements were defined as for NOMAD. The camera could be moved independently along the three axial directions, with a crosshair on the monitor screen indicating the center of the field of view of the camera.
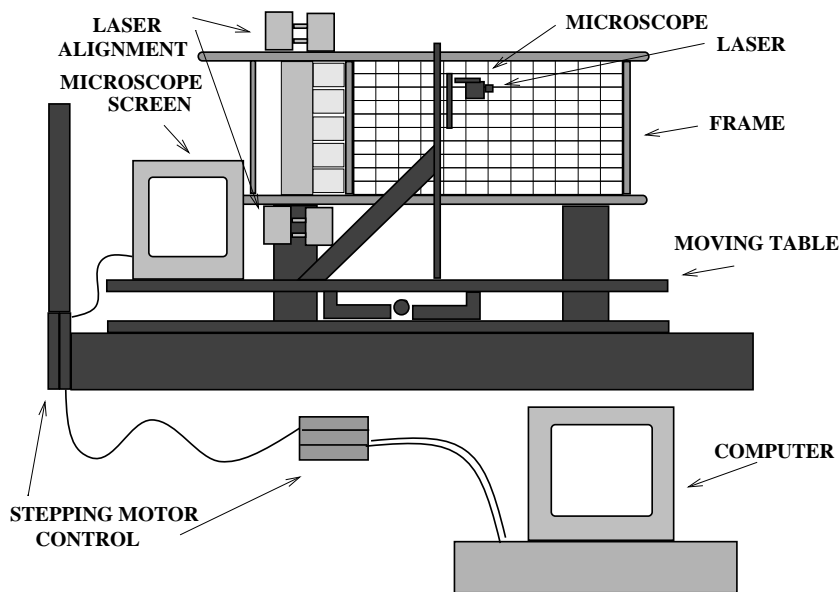

Figure 14: System used for surveying the layers of NOMAD–STAR.

The camera could be moved by stepping–motors in increments of 1 μm, although the precision of the measurements was limited by the quality of the image and the precision of the movement. A PC was used to control and read the position display and store the measurement data to a file.

To measure the X- and Y-coordinates of a point, the camera was focused and the monitor crosshair positioned on the target. A distinctive feature of the measurement bench was the Z–reference. A red laser, oriented at 45° to the camera, was focused on the surface to be measured. A spot could be seen on the monitor if the laser light reflected diffusely from an aluminized surface of the detector. The camera was adjusted in the Z–direction so that the center of the laser spot coincided with a crosshair on the monitor screen. The crosshair was adjusted *a priori* so that the camera was in focus when the laser spot was centered at the crosshair.

Four points were measured per detector, giving a total of 48 points per ladder. Each ladder was measured by at least two different surveyors to check for any discrepancies. In the rare cases in which discrepancies were found, the estimated theoretical position of the detectors was used to determine which of the two measurements was at fault.

A final survey was performed with the silicon frames mounted in the final support structure (mini–basket, see section 7).

6.1 Survey Results

The resolution of the surveying system is shown in Figs. 15a, 15b and 15c. The resolution in X and Y are $\sigma_x \sim 6$ μm and $\sigma_y \sim 7$ μm from the knowledge of the detector length and height, respectively. The resolution for the Z–coordinate is $\sigma_z \sim 14$ μm, based on the reproducibility of measurements performed by different surveyors. The systematic uncertainty in the X-, Y- and Z-positions was determined from the reproducibility of the results from different operators and on comparisons of results with the layers before and after installation inside the mini-basket. These were: $\sigma_x \sim 6$ μm, $\sigma_y \sim 7$ μm and $\sigma_z \sim 31$ μm.

The individual detector positions were converted into the NOMAD reference system through external surveyor measurements. The positions of each of the detectors inside the NOMAD reference system determined in the manner described above will act as seeds for an *in situ* alignment process that will be done using muons from the muon gate of the SPS cycle.

7 Support system and cooling

The 10 silicon ladders of each plane are mounted on an aluminum frame as shown in Fig. 3. Cooling pipes with demineralized water run around the frame and along the electronics. This allows to keep temperature variations below 0.5°C at the normal operating temperature of 22°C. The power dissipation per silicon plane is around 20 W. The 5 silicon planes are fixed with dowel pins into an aluminum support, the mini–basket. The mini–basket has 4 external survey marks which were used as reference points for the final survey of the silicon detectors. The mini–basket is suspended from a global support structure at the NOMAD experiment as shown in Fig. 16. The B_4C target plates are suspended independently from the general support structure and are lowered in place by a system of pulleys with lead counterweights. Two scintillator counters upstream of the target act as a veto (V_S) for incoming charge particles. Two scintillator counters downstream of the target act as a trigger (T_S) for interactions in NOMAD–STAR (see section 9.3). All four scintillator triggers are suspended independently from the general support. The general support has survey points at the top, which remain visible once installed in the experiment. Prior to installation at the experiment,
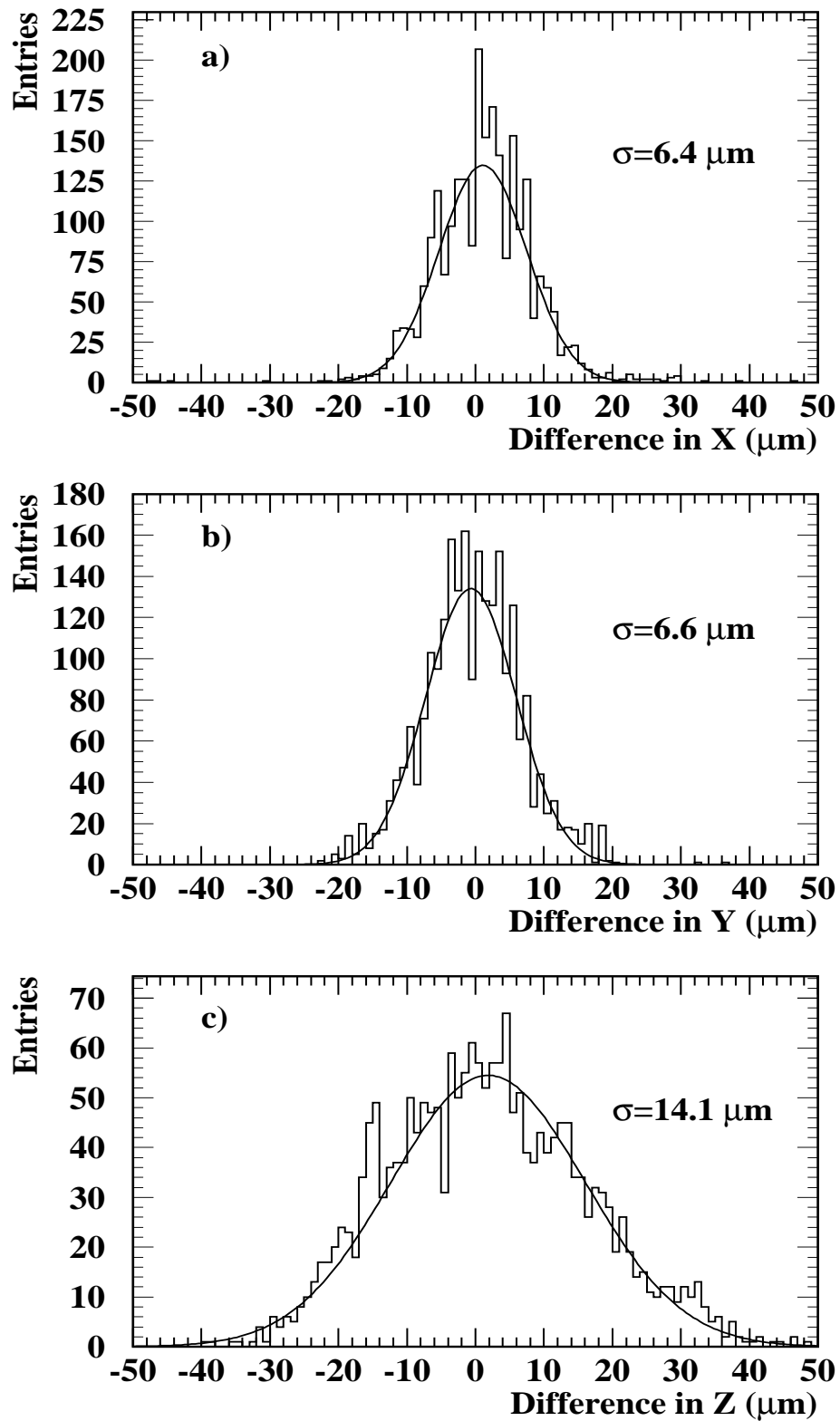
Figure 15: Resolution of the surveying system. Systematic differences in the measurements of the coordinates a) X, b) Y and c) Z.
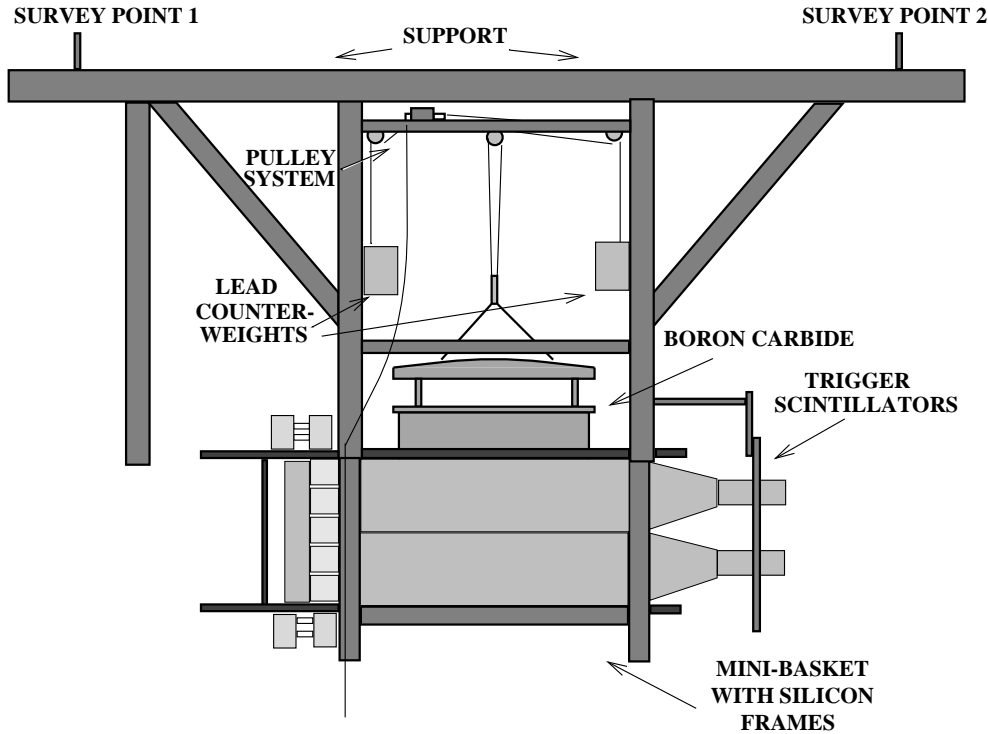
Figure 16: Support system for NOMAD–STAR with mini-basket and silicon layers.

the external survey marks of the mini–basket were aligned with respect to the survey points of the general support. To make space for the B_4C–silicon target module, the first three target drift chambers of the NOMAD experiment had to be removed.

8   The Front-End Electronics

8.1   Overview

NOMAD–STAR requires the use of very low noise electronics operating at large peaking times (2-3 μs).

8.2   Readout Chips

We used the VA1 readout chip[11] which consists of 128 charge sensitive, low–power (1.2 mW/channel) and low–noise preamplifiers followed by CR–RC shapers, track–and–hold circuitry, output multiplexing and a multiplexing calibration circuit.

As shown in equation (1), the VA1 readout chip is very suitable for ladders with large input capacitances [11].

$$\mathrm{ENC}_{VA1} = 169e^- + 5.6\mathrm{e}^-\mathrm{C}_t/\mathrm{pF}, \tag{1}$$

---

[11]A commercial version of the VIKING chip [15] manufactured by IDE AS, Norway.

The total noise for a typical ladder was of the order of 1400 *rms* electrons, corresponding to a signal–to–noise ratio of about 16. A detailed description on the chip performance with the NOMAD–STAR ladders is given in [11].

8.3 Hybrid Printed Circuit Board

Five VA1 chips are mounted onto a hybrid card[12]. It consists of a multilayer printed circuit board glued onto a ceramic substrate (Al_2O_3) which contains a connector and surface mounted devices (SMD). The VA1 chips were delivered separately and were glued and aligned with a precision better than 50 μm. The hybrid houses clock and test mode lines for the VA1 chips and bias lines for the detectors.

8.4 Repeater Cards and Mother Boards

The sequential output signals are amplified on a repeater card which also drives the clock signals to the hybrid and allows adjustment of various voltages controlling the operation of the VA1 readout chip.

Each repeater reads 1280 channels (2 ladders which are read out in series). The output signals for five repeaters are routed to a printed circuit mother board and transported over a 30 m–shielded twisted pair cable to five flash ADC channels(see section 9.2).

The readout electronics require $\pm$ 6 V for the amplifiers and $\pm$ 2 V for the VA1. Each of the 25 repeaters has a voltage regulator from which the $\pm$ 2 V needed to power the readout chips are derived. Thermistors are located near the voltage regulators where most of the heat is being dissipated.

9 Data Acquisition

9.1 Overview

The layout of the silicon readout system, is based on a VME Local System Crate. The Local System Crate controls the silicon readout and also communicates with the NOMAD trigger and readout system. The silicon system consists of 32,000 analog channels. An online program and the slow-control continuously monitor NOMAD–STAR during the data-taking period.

---

[12]Also manufactured by IDE AS, Norway.

9.2 The Sequencer and ADC modules

The sequencer and ADC modules[13] are controlled through a VME bus. Detector channels are read out by V550 flash ADC modules accepting up to 2×2016 channels, and timing signals are provided by a V551B Sequencer.

Following an external event trigger, readout clock signals are generated by the sequencer unit. The hold level is asserted and the sequential readout is performed by activating the output shift registers, using a clock operating at a frequency of 1 MHz, and shift–in/shift–out signals. Optimal noise performance has been obtained for a shaping time of 3 μs [11].

The maximum readout clock frequency is 5 MHz, but a deterioration of the signal was observed at frequencies larger than 4 MHz. A single NOMAD–STAR trigger can be read out for each neutrino spill (5 ms). The trigger rate is about 0.2 per neutrino spill nad therefore the limitation of being able to read only one NOMAD–STAR event per spill does not reduce significantly the accepted number of events. For each SPS accelerator cycle (14.4 s) there are two neutrino spills at a 2.4 s interval.

9.3 Trigger and Data Processing

To reduce costs, the NOMAD–STAR detector readout is implemented in a very simple manner. Stringent trigger requirements are necessary to maximize the probability that the recorded events correspond to neutrino interactions in the NOMAD–STAR detector. The trigger for NOMAD–STAR, is a coincidence of the following signals:

- $\overline{V_8}$, the central part of the NOMAD veto (see Fig. 1), to eliminate incoming charged particles,

- $\overline{V_S}$, two scintillators just upstream of NOMAD–STAR, to eliminate neutrino interactions in the front part of the NOMAD magnet,

- T_S, two scintillators just downstream of NOMAD–STAR, to signal the presence of charged particles exiting the detector, and

- T_1, one of the two NOMAD trigger scintillator planes, ensuring, with T_S, that some of the charged tracks resulting from an interaction in NOMAD–STAR pass through most of the NOMAD tracking volume.

When such a trigger occurs, further NOMAD–STAR triggers are inhibited for the remainder of the neutrino extraction and the readout procedure commences. 128 strips are connected to each readout chip, and ten of these chips are read out on a single ADC channel. Each of the twenty-five ADC channels uses serial multiplexing to read out its corresponding strips. Each ADC does this independently taking

---

[13]Manufactured by CAEN, Italy.

about 1.3 ms to receive the data. For ease of calculation offline, the pedestals are all subtracted inside the ADC modules with zeros being subsequently suppressed. The negative values are kept for common–mode noise calculation which the ADC module cannot perform. The twenty-five ADC channels are located on thirteen VME 6U cards (CAEN V550 CRAMS), each of which is read out by a central CPU via block transfers. This transfer requires approximately 10 ms. The resulting data is then formatted with address and error information being added before it is passed on the event–building part of the data–acquisition and finally written to tape. The NOMAD–STAR neutrino triggers normally represent less than 5% of all neutrino triggers accepted, although they represent close to 25% of the data volume in the neutrino gates since the suppression of inactive channels is only performed offline. The statistics obtained are sufficient to enable measurement of the viability of silicon as a detector for accelerator-based neutrino experiments; the statistics are not sufficient, however, to perform any fundamental physics measurements.

In conjunction with the rest of the NOMAD detector, the NOMAD–STAR detector also accepts triggers coming from muons which are generated upstream of the experiment during the 2.4 second period in–between the neutrino extractions. The trigger is similar to the neutrino trigger described above, except that the two sets of veto counters are placed in coincidence, rather than in anticoincidence. Normally, two to five muon triggers are accepted per cycle.

9.4   Monitoring

For the neutrino and muon gates the online program displays the hit multiplicity in each silicon layer, the position of hits and their corresponding charge deposition. In addition, the cluster multiplicity and resolution are calculated for each of the five silicon layers. In the calibration gate ($\simeq 12$ s), pedestal, noise, and common–mode shift distributions are calculated for every readout chip.

9.5   Slow Control

In addition to providing information on the status of the detector, protective measures such as alarms, software cuts and hardware cuts are implemented in the slow control. These are designed to prevent the detector from being damaged due to malfunction.

The most important parameters to be monitored are the temperatures on the hybrids as these are most susceptible to damage. A thermistor is used to measure the temperature on each of the 10 hybrids in a given silicon layer. Typical values are approximately 23 °C. Temperatures on repeaters are also monitored, with typical values being approximately 29 °C. In addition, temperatures in two different places on the support frame that hosts the detector (mini–basket) are measured. Typically 22 °C is attained at these points.

The leakage currents and the 60 V reverse–bias voltage are measured per repeater, i.e. two ladders at a time. The ± 2 V and their corresponding currents necessary to power the readout chips are also monitored. Finally, the voltages required by the laser alignment system (see section 10) are also monitored. Additional sensors monitor the water cooling system.

If the temperature of a hybrid rises above a certain value, a software cut is applied on the low–voltage of the electronics, operating on a hybrid–by–hybrid basis. Hardware cuts are applied through a veto module in the electronics crate of NOMAD–STAR and are used if the temperature on a repeater rises above a certain level. This causes the low–voltage for the entire plane of the repeater to be cut. If temperatures on the repeaters of all layers are beyond a given threshold, the 60 V high–voltage and the low–voltage for the electronics are cut for the entire detector. Thermistor readings are stored on tape for each data taking run (typically 2 hours).

10   Laser Alignment System

In order to monitor *in situ* any relative movements of the silicon ladders, a laser alignment system based on twenty semi–transparent position sensitive sensors is used. A detailed description can be found elsewhere [16]. Four sensors (2 for X–position and 2 for Y–position measurements) were mounted rigidly on each of the five aluminum frames which provide the mechanical support for the ladders.

Figure 17 shows the position resolution of a typical sensor to be 1.5 μm. Readings from the sensors are taken at the start of each run, typically every 2 hours

11   Conclusion

We have described the construction of a B_4C–silicon target for the detection of neutrino interactions.

The passive material has a total mass of 45 kg and the ladders of silicon detectors are 72–cm long. A silicon detector yield of 96% was obtained. A typical silicon ladder has a signal–to–noise ratio of 16, 1.4% defective channels and a leakage current of about 2 μA. The silicon detectors have been aligned with a precision better than 10 μm in the plane perpendicular to the beam direction.

The target was installed in the NOMAD spectrometer at the CERN SPS neutrino beam, and about 8000 ν_μ charged current interactions were estimated to have occurred in the target during the 1997 run. The construction of the target and the analysis of its data will provide invaluable experience towards the construction of a future large scale silicon tracker for neutrino oscillation
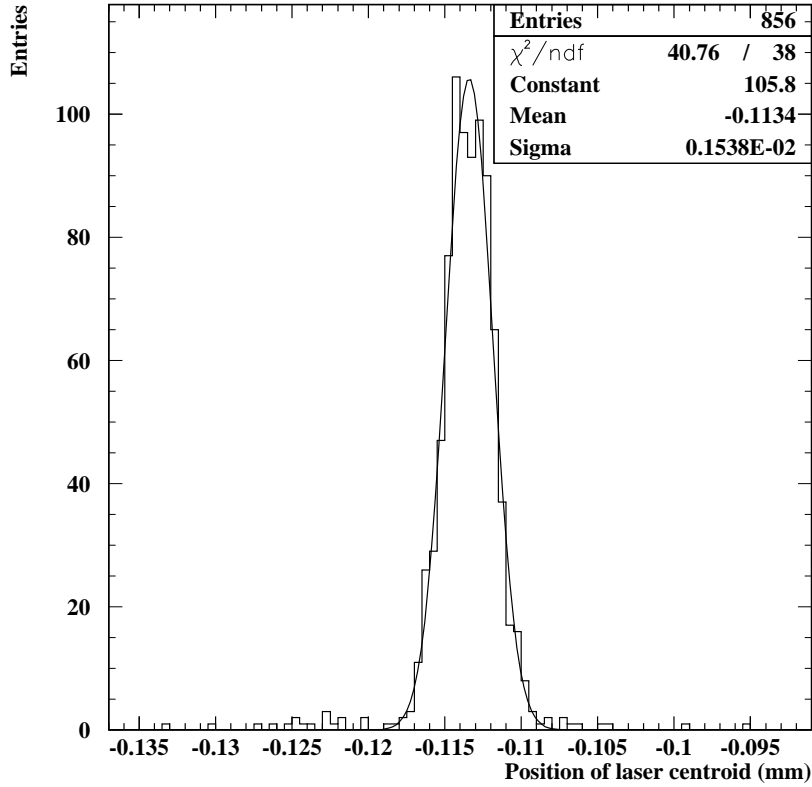
Figure 17: Position resolution for a typical sensor used in laser alignment system. The width of the distribution corresponds to the resolution of the sensor (1.5 μm).

experiments.

Acknowledgements

References

[1] CHORUS Collaboration, E. Eskut *et al.*, Nucl. Inst. and Meth. **A401** (1997) 7-44.

[2] NOMAD Collaboration, J. Altegoer *et al.*, *The NOMAD Experiment at the CERN SPS*, CERN-PPE/97-59 26 May 1997. Submitted to Nucl. Inst. and Meth.

[3] J.J. Gomez-Cadenas, J.A. Hernando and A. Bueno, Nucl. Inst. and Meth. **A378** (1996) 196.

[4] J.J. Gomez-Cadenas and J.A. Hernando, Nucl. Inst. and Meth. **A381** (1996) 223-235.

[5] A. Ereditato, P. Strolin and G. Romano, *Study of a new experiment for the search of muon neutrino and tau neutrino oscillations*, CERN-PPE-96-106, June 1996; Nucl. Phys. Proc. Suppl. **54B** (1997) 139-150.

[6] A.S. Ayan *et al.*, *A high sensitivity short baseline experiment to search for $\nu_\mu \leftrightarrow \nu_\tau$ oscillation*, CERN-SPSC/97-5, SPSC/I213, March 1997.

[7] J.J. Gomez-Cadenas, *Towards a Next Generation $\nu_\mu(\nu_e) \leftrightarrow \nu_\tau$ Oscillation Search Experiment*, Proceedings of the Faro Workshop, Faro, Portugal, September 1996. To be published by World. Sci. eds.

[8] K. Kodama *et al.*, *Muon–neutrino to tau–neutrino oscillations: PROPOSAL*, FERMILAB-PROPOSAL-P-803, October 1993.

[9] A. Zalewska, *The Silicon Tracker in the DELPHI Experiment at LEP2*, EPS–HEP Conference, Pa 17, Jerusalem, 19–26 August, 1997.

[10] P.P. Allport *et al.*, Nucl. Inst. and Meth. **A 310** (1991) 155.

[11] G. Barichello *et al.*, *Performance of Long Modules of Silicon Microstrip Detectors*, CERN-PPE 97-162, 11 December 1997. Submitted to Nucl. Inst. and Meth.

[12] Ö. Runolfsson, Nucl. Inst. and Meth. **A 383** (1996) 223.

[13] Hamamatsu Photonics Inc., private communication.

[14] A. Cervera-Villanueva *et al.*, *Survey of the Frames for STAR*, NOMAD Internal Note, NOMAD-MEMO-97-48, 18 December 1997.

[15] O. Toker *et al.*, Nucl. Inst. and Meth. **A 340** (1994) 572.

[16] H. Kroha, Nucl. Phys. Proc. Suppl. **54B** (1997) 80;
W. Blum, H. Kroha and P. Widman, Nucl. Inst. Meth. **A377** (1996), 404;
W. Blum, H. Kroha and P. Widman, Nucl. Inst. Meth. **A367** (1995), 413.